JOURNAL OF MATERIALS SCIENCE 8 (1973) 1603–1615

The microstructure of hot-pressed silicon-nitride

RAM KOSSOWSKY
Materials Science Section, Metallurgy and Metals Processing Department, Westinghouse Research Laboratories, Pittsburgh, Pennsylvania, USA

Grain morphology, distribution of impurities and inclusions, phases and dislocation structures in two grades of hot-pressed Si_3N_4 were investigated by means of replica and thin foil transmission microscopy, and by X-ray diffraction, microprobe and Auger analyses. High concentrations of impurities, specifically Ca, were detected at the grain boundaries. Fe-W-Si particles were seen within the grain. Non-densified Si_3N_4 inclusions were found to be detrimental to the strength. Possible correlations among strength, densification data and distribution of elements and phases are discussed.

1. Introduction

The microstructure of hot-pressed Si_3N_4 was previously discussed by Evans and Sharp [1] and by Butler [2]. These authors were mainly concerned with the crystallography [1] of the material and the dislocation characteristics [1, 2]. In the course of an extensive study of the mechanical behaviour of the material [3, 4], it became apparent that impurities, inclusions, grain boundaries, grain morphology and dislocation structures are important factors that control the mechanical behaviour of Si_3N_4. Specifically, these effects become prominent at elevated temperatures (above 1000°C) where the material is intended for extended service in gas turbine applications.

The purpose of this paper is to report what we believe is the first comprehensive examination of the microstructural aspects of hot-pressed Si_3N_4. Where possible, the effects of the structural parameters on strength are pointed out. More comprehensive studies of the effect of inclusions, impurities and grain-boundary structure on the high temperature strength and creep behaviour of Si_3N_4 are being carried out to extend the present investigation and the results will be published in the near future.

2. Experimental procedure

Two grades of Si_3N_4, designated HS-110 and HS-130, respectively, were received from the Norton Company in the form of hot-pressed billets, 150 × 150 × 25 mm thick. After grinding off the rough crust, samples were cut from various locations within a given billet, and specimens were prepared for the following examinations.

2.1. Chemical analysis and X-ray powder diffraction

Samples were crushed using a tungsten-carbide mortar and pestle. For W analysis, samples were prepared using BN balls. Spectrographic analysis was performed on eleven different billets. Two samples were taken at random from each billet (avoiding the end layers), and duplicate tests were run on each sample. Concentrations of up to 0.1 wt % were read automatically from an RSV direct-reading 3.5 m spectrometer and converted to wt % from previously prepared calibration charts. The accuracy of this method is estimated at ± 50% of the read value. In most of the cases the variances in the duplicate readings were within the accuracy range. When the variance was higher, the results were discarded and new samples were prepared for analysis. Elements with concentrations of more than 0.1% were read visually from glass plates obtained in a photographic, Jarrel-Ash 3.4 m instrument. The accuracy of this method is estimated to be 0.3 to 3 times the read value.

2.2. Grain morphology and microprobe analysis

Specimens were mounted in "Kold" mount and rough polished with 600 grit paper. Final

© *1973 Chapman and Hall Ltd.*

polishing was done on cloth with "Linde B" solution. The specimens were removed from the "Kold" mount, pre-heated and etched at 740°C in a eutectic mixture consisting of 93 g K_2CO_3 and 15 g NaF [5]. 1 min etching time was found to yield the best results. Surface replicas were then prepared using two-stage carbon replication shadowed with a gold-palladium alloy.

2.3. Auger analysis

Specimens of square cross-section, 2.5 mm on the side, were placed in the vacuum chamber, which was evacuated overnight to more than 10^{-9} Torr. The specimens were then fractured, thus exposing a virgin fractured surface. Extensive examination of a large number of fracture surfaces indicated [3, 4] that the fracture is predominantly intergranular at all temperatures including room temperature, and is thus expected to expose a high percentage of grain-boundary area.

Reduction of the data in terms of semi-quantitative values was obtained by measuring the peak-to-peak height (I_x) of the major peak of each element present. From the known relative sensitivity, S_x, of each element with respect to an Ag standard, and the scale factor, K_x, the concentration of element x in at. % is given by [6]

$$C_x = \frac{I_x 100}{S_x K_x} \Big/ \sum \frac{I_a}{S_a K_a} \qquad (1)$$

where the sum is over one peak from each element present on the surface.

2.4. Thin foil transmission

6 mm wide and 1 mm thick strips were sliced off the billet with a diamond wheel. The strip was placed on a glass slide and ground down to 0.05 mm thickness. 3 mm diameter discs were cavitated from the strips and placed in an ion-beam milling machine for thinning to perforation at a beam current of 100 μÅ, 6 kV potential and a tilt of 15°. The foils were examined at 800 kV, in an RCA 1000 kV microscope and also at 100 kV in a Phillips EM-200 microscope.

3. Results

3.1. Chemistry

Spectrographic analyses of one billet of the HS-110 material and variations within ten billets of the HS-130 material are shown in Table I.

Most of the impurities can be traced to the starting silicon powder; a few are added during the process of hot-pressing. Mg is added as MgO, to promote liquid phase sintering [1, 7]. The high concentrations of W are a result of prolonged ball milling with WC* balls, which is probably the major source of carbon, also. The reduced levels of W in some of the billets could be due to a change in the milling process or to a separation schedule. Fe additions are known to promote fast and efficient nitriding of silicon powder [8].

3.2. Grain morphology

A replica transmission micrograph of a polished and etched sample of HS-130 grade Si_3N_4 is shown in Fig. 1a. A thin foil transmission micrograph of HS-110 grade is shown in Fig. 1b. Both samples were removed from the short face of the respective billet so that the hot-pressing direction is vertical and lies in the plane of the micrograph. Similar micrographs were obtained from samples removed from the other two faces of the billet.

A bimodal distribution of grain sizes was measured, Fig. 2. About 80% of the grains are equiaxed, and vary in size between 0.5 and 3 μm, with an average size of 1.3 μm. The other 20% of the grains have an elongated appearance, with the short axis between 1 and 2 μm and the long axis between 2 and 5 μm. Both types of grains have been identified by electron diffraction

TABLE I Spectrographic analysis, hot-pressed Si_3N_4 (wt %)

Billet No.	Al	B	Ca	Cr	Fe	K	Mg	Mn	Na	Ni	Ti	W	C
011072 B1 (HS-110)	0.8	0.01	0.5	0.2	0.6	0.01	0.6	0.02	0.01	0.01	0.01	~3	0.41
HS-130	0.07–0.12	0.001	0.02–0.08	0.04	0.7–0.1	0.004–0.007	0.7	0.04	0.003–0.02	0.01	0.02	0.3–3	0.43–0.04

Accuracy: W and Fe by visual reading; accuracy 0.3 to 3 times amount present.
All other elements by direct reading; accuracy ± 50% of amount present.

*Since details of the manufacturing process are not available, our comments are based on the patent literature and the work of Lange and Terwilliger[5] [5].

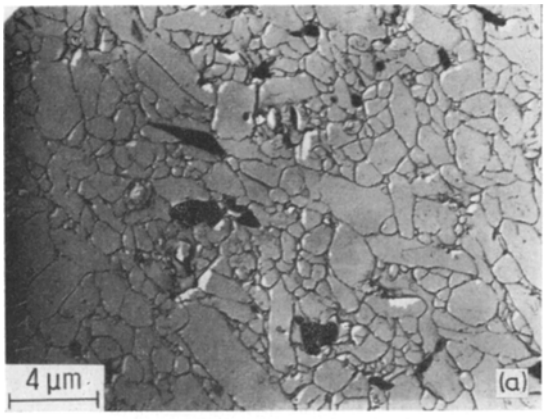

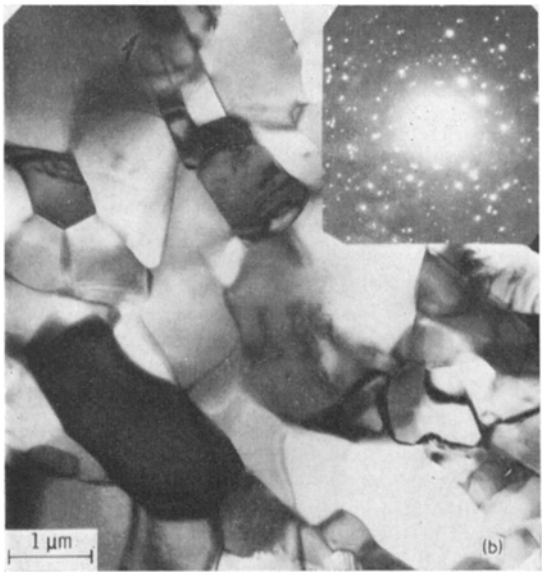

Figure 1(*a*) Replica transmission micrograph polished and etched surface. HS-130 grade Si_3N_4. Hot-pressing direction vertical.
Figure 1(*b*) Thin foil transmission electron micrograph. HS-110 grade Si_3N_4.

as the β phase [1] of Si_3N_4. About 1% of the elongated grains are larger, up to 20 μm long. These grains were identified as the α phase [1] of Si_3N_4.

X-ray radiography showed variations in intensity which indicate layers of varying density. These layers are perpendicular to the hot-pressing direction and may be attributed to a combined result of bad mixing and gradients in pressure along the pressure axis. The boundaries between the layers could be a source of lower strength, when the applied stress is normal to these boundaries.

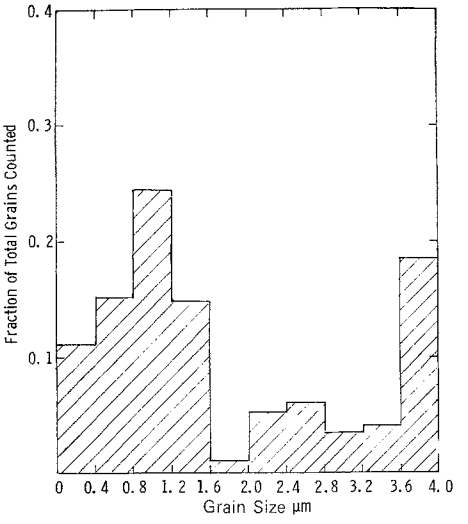

Figure 2 Histogram of grain size distribution, hot-pressed Si_3N_4.

Lange and Terwilliger [5] suggested that preferred orientation of elongated grains exists in the hot-pressed billet. Micrographs similar to Fig. 1 were obtained from all three faces of the billet without any apparent visual difference. Nevertheless, pole-figure analysis indicates some preferred orientation. Fig. 3 is a reproduction of a (210) pole-figure. The hot-pressing direction is vertical. The pole-figure (Fig. 3a) and the histograms (Fig. 3b) show that about 15% of the grains are oriented, with the basal planes within 20° of the hot-pressing direction, or conversely, with the C-axes within 70° of the hot-pressing direction.

3.3. Inclusions and impurities

Occasionally found inclusions are shown in Fig. 4, which shows micrographs of the fracture surfaces of three flexural specimens. These specimens were selected from a group of twenty tested in a four-point bend mode in air at 1000°C. The average strength of this group was 475 MN m^{-2} (standard deviation $\pm$ 48.2 MN m^{-2}) and as shown in Fig. 4, the decrease in strength owing to the presence of an inclusion could amount to as much as 35%.

An inclusion of free silicon is shown in Fig. 4a. In this particular case the particle is located below the highest stressed tensile surface. The micrograph clearly indicates that failure originated at the particle-matrix interface.

Another, infrequently observed inclusion is an

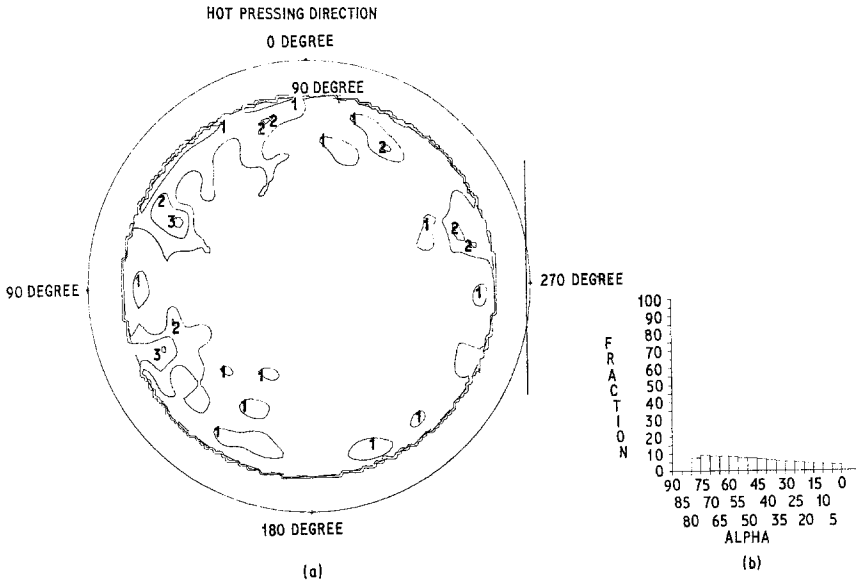

Figure 3 (210) pole-figure analysis. (a) Hot pressing direction vertical. (b) Histogram of sums of X-ray intensities at 5° interval circle on a 360° rotation around the (210) axis. Oriented grains between the 65° and 75° concentric circles.

iron-rich particle, as shown in Fig. 4b. A rarely found inclusion is shown in Fig. 4c, which depicts a magnesium rich particle, located at the bottom of a round hole.

Extensive X-ray radiography* was conducted on flexural test specimens in an attempt to correlate detectable flaws with strength degradation. Groups of ten specimens from five different HS-130 grade billets were radiographed. Two types of defects were observed, i.e. low density spots and high density particles. After testing all fifty specimens, it was quite obvious that the majority of the fractures in specimens tested both at 1000 and 1300°C were *not* associated with high density spots. On the other hand, in *most* of the specimens that failed at stresses below the standard deviation range of the respective group, a white, low density, powdery particle was found to be associated with the origin of fracture.

Microprobe traces taken across these inclusions showed a lower concentration of Si than in the bulk and non-uniform occasional bursts of carbon that were about twice as high as in the bulk. A few of the inclusions were removed using a WC tool and subjected to a Debye-Scherer X-ray diffraction. Faint lines, corresponding to hexagonal BN, were seen along with strong lines from β-Si_3N_4. Laser-source emission spectroscopy showed that some of the inclusions contain a fair amount of B. We suggest, therefore, that the white powdery inclusions are small pockets of non-densified mixture of Si_3N_4 and BN powders. This was confirmed by examining the inclusions in the scanning electron microscope. BN is used to coat the walls of the graphite die in which the billet is hot-pressed. It is quite probable that some of the BN powder is admixed during die filling. The BN powder that is rubbed off the die wall could also account for the carbon that is found in the inclusions.

Fig. 5 shows typical fracture surfaces containing the white, non-densified inclusions. Fig. 5a is from a flexural specimen machined so that the tensile axis was parallel to the hot-pressing direction, while the specimen shown in Fig. 5b was machined with the tensile axis normal to the hot-pressing direction. The micrographs show that these inclusions are associated with the source of fracture [9] marked by the area of slow crack growth [10], and that the apparently spherical inclusion is squashed to a lenticular shape during hot-pressing.

The distribution of major impurity elements

*Test performed at the Army Materials and Mechanics Research Center, in co-operation with Dr R. Katz and Mr S. Der Boghosian.

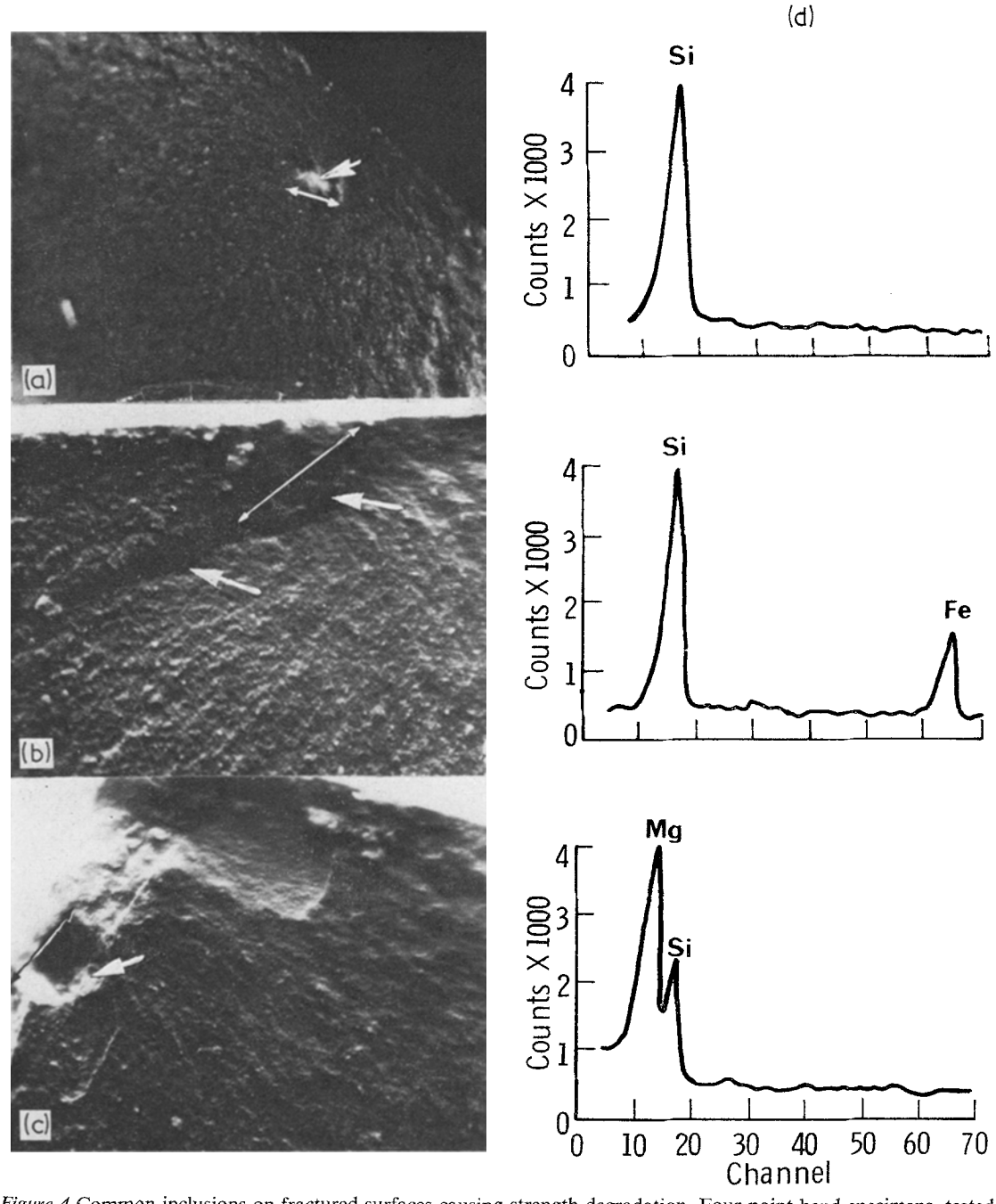

Figure 4 Common inclusions on fractured surfaces causing strength degradation. Four point bend specimens, tested at 1000°C Average strength (twenty specimens) 475 MN m^{-2} (a) Free silicon inclusion failed at 276 MN m^{-2} light micrograph (× 35). (b) Iron-rich inclusion. Failed at 315 MN m^{-2} SEM micrograph (× 130). (c) Mg-rich inclusion. Failed at 398 MN m^{-2} SEM micrograph (× 140). (d) Energy dispersive X-ray analysis at indicated spots.

was examined by Auger and microprobe analyses. The results of the Auger analysis for both grades of Si_3N_4, are shown in Fig. 6.

The reliability of the analysis is demonstrated by comparing, in particular, the Al, Fe and Mg profiles to the spectrographic analysis. Since these elements seem to be concentrated in the grain at least as much as in the grain bound-

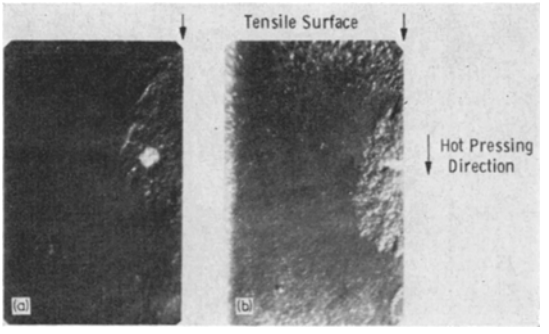

Figure 5 Light micrographs showing orientation of lenticular, non-densified Si_3N_4 inclusion in flexural test specimens with respect to hot pressing direction (× 10). (a) Hot-pressing direction normal to plane of figure, and parallel to tensile axis. (b) Hot-pressing direction vertical and normal to tensile axis.

TABLE II Concentration of elements in wt %, within the grain in Si_3N_4
Data Converted from Auger Profiles, Fig. 6

	Si	N	O	Fe	Al	Mg	Ca
HS-110	balance	34	8	1.2	1.4	0.9	0.8
HS-130	balance	36	6.5	1.2	—	0.7	—

aries, the levels of Fe, Al and Mg following extensive sputtering should compare to the bulk composition. A comparison of Tables I and II shows a close agreement between the two analytical results. One should further note the somewhat higher reading of oxygen in the HS-110 material, compared to the HS-130 (Table II). Bulk compositions, obtained by neutron activation analysis [11], show a range of 2 to 5 wt % of oxygen in the HS-130 grade and 6 to 9 wt % of oxygen in the HS-110 grade.

The high readings of oxygen after the prolonged sputtering are probably contaminations from the argon gas. The high concentrations of oxygen at the grain boundaries are consistent with the existence of a boundary glass phase [7], though transmission micrographs of the Norton material did not positively show the grain-boundary phase.

Results of microprobe analyses are shown in Figs. 7 and 8. Since the beam diameter is one of the order of the grain size, it was possible to resolve with some degree of certainty, the mode of distribution of the impurities only when a large grain was located. Fig. 7 shows scans of five elements over an area in which a few large grains are located. Fe and W are concentrated in the same area; this was confirmed by examining many scans of these two elements. The Fe-W rich clusters are about 10 μm in diameter and lineal analysis of low magnification scans showed that they occupy about 3% of the volume.

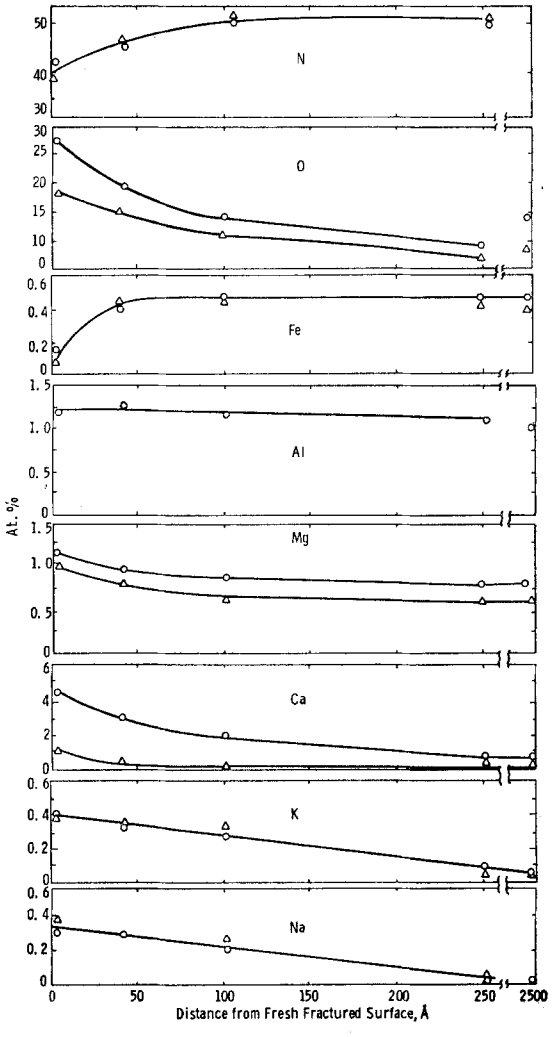

Figure 6 Elements distribution profiles, hot-pressed Si_3N_4 Auger analysis. 0: HS-110 grade, Δ: HS-130 grade.

Fig. 8 shows line traces of six elements taken along the dotted line marked in Fig. 7a. The overlap of the Fe and W peaks is obvious. There is a decrease in the Mg content across the large grain, and a small but a finite increase in Al across the same area. The probe results are in good agreement with the Auger analysis and confirm the concentrations of Fe and W within the grain.

Impurity distributions on a microscopic scale

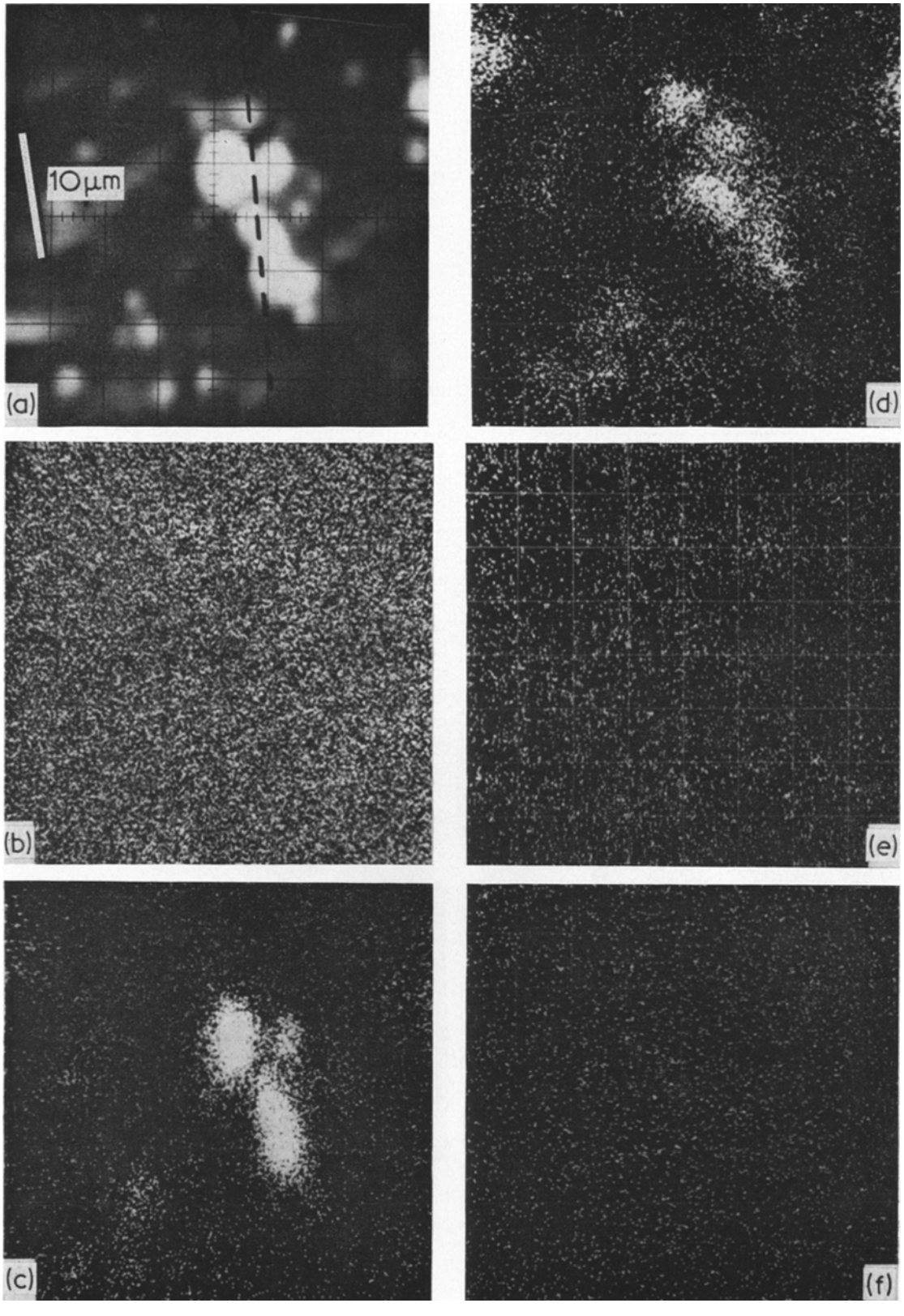

Figure 7 Microprobe scans, HS-130 hot-pressed Si_3N_4 (a): Back scattered electrons, (b): SiK_α, (c): WM_α, (d): FeK_α, (e): MgK_α, (f): CaK_α.

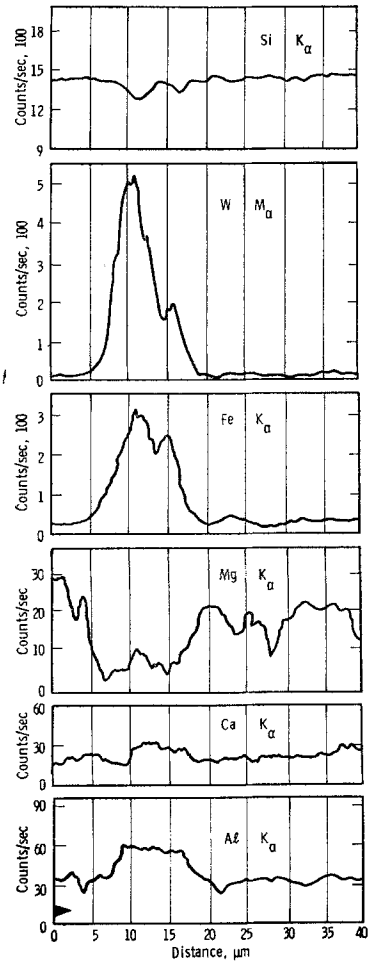

Figure 8 Microprobe traces of impurity elements in HS-130, hot-pressed Si_3N_4. Direction of trace marked in Fig. 7a.

are shown in Fig. 9. Fig. 9b shows a cluster of semi-coherent particles within a large grain. Although the diffraction patterns show extra spots (arrows), positive identification was not possible. One should note the strain fields that are associated with these particles. The strain fields are apparently a result of differential thermal contraction between the particles and the matrix during the cooling cycle following hot-pressing.

About a dozen samples were examined by Debye-Scherer X-ray diffraction. Apart from weak traces of Si_2ON_2 in the HS-130 material, only the β phase was identified in both grades of Si_3N_4. Metallic elements or phases, such as indicated by the Auger and probe analyses, and the transmission micrographs, were not identified.

3.4. Dislocations

Typical dislocation networks present in hot-pressed Si_3N_4 are shown in Fig. 10. The top row shows dislocations in rarely found α grains, while the bottom row shows dislocations in β grains. These observations are in general agreement with the dislocation structures reported by Evans and Sharp [1] and by Butler [2], which were confirmed to β grains only. Fig. 10 shows that there is, essentially, no difference in the dislocation structures in both phases. Generally, the dislocation density is low, and most dislocations are associated with loose networks and slip bands. Occasionally, a dense tangle (Figs. 10b and d) is observed which is traced to a severe localized deformation during hot-pressing [1].

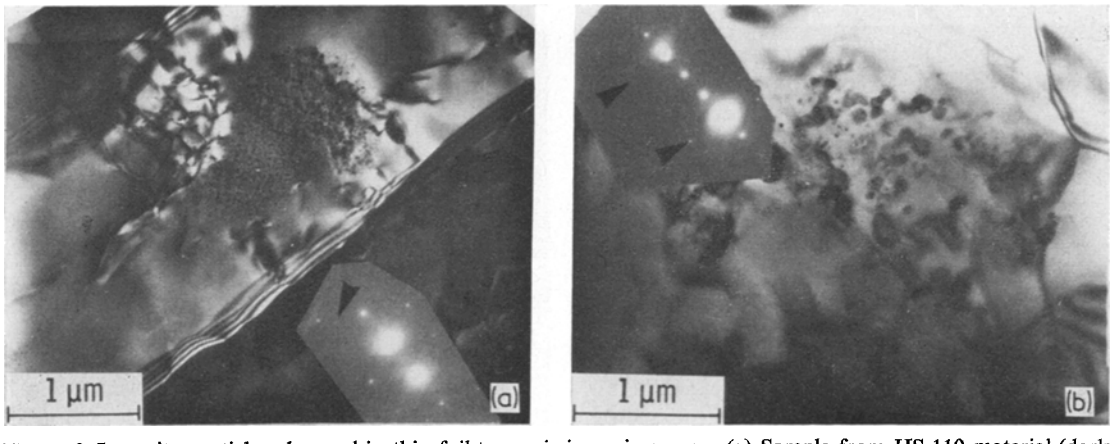

Figure 9 Impurity particles observed in thin foil transmission microscopy. (a) Sample from HS-110 material (dark field off main spot). (b) Sample from HS-130 material. Note strain fields associated with particles in (b). Arrows indicate extra spots, probably due to particles.

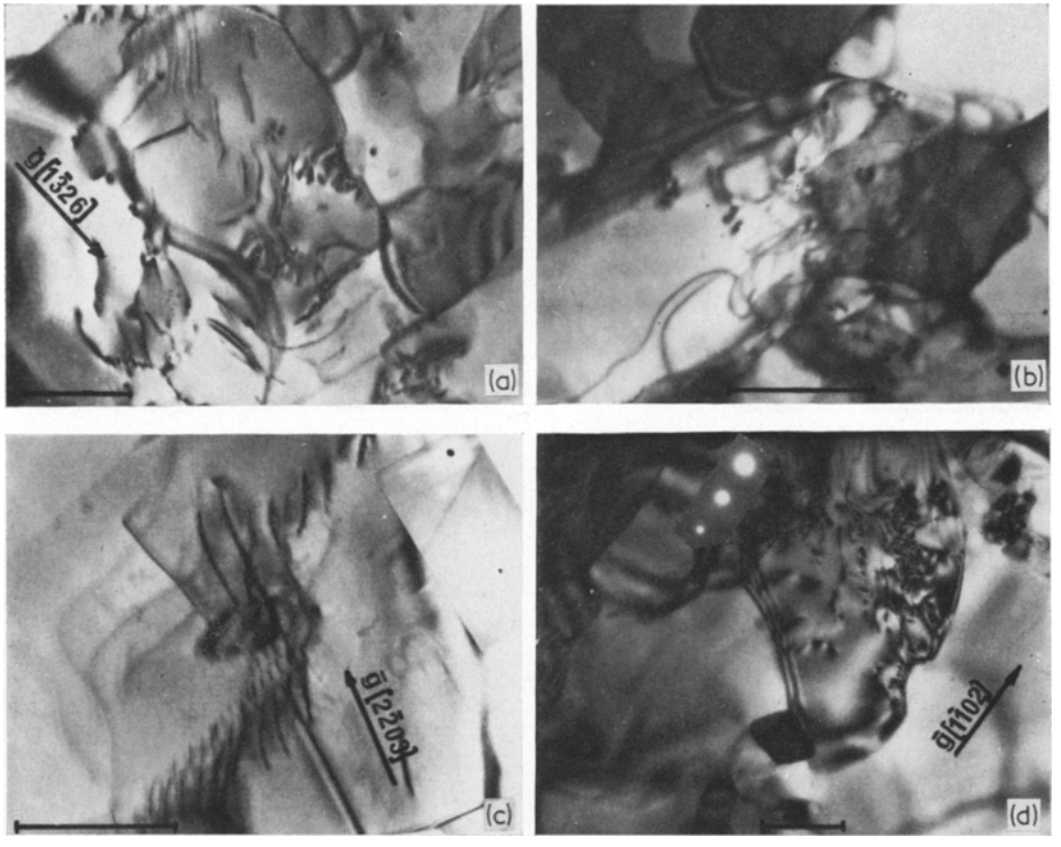

Figure 10 Dislocations in hot-pressed Si_3N_4. (a) Typical low density in a large α grain. (b) Occasional tangle in an α grain. (c) A pile-up of screw dislocation. Large β grain. (d) Occasional tangle, β grain. 0.5 μm scale bars.

More prominent, however, are grain-boundary dislocation networks and low-angle boundaries [2], shown in Fig. 11. A twist boundary and a pile-up at the boundary are shown in Fig. 11a. Low-angle boundaries are visible clearly in Fig. 11c. Moiré patterns, typical of low angle boundaries, are seen in Figs. 11b and d. Owing to the small grain size it was difficult to obtain single diffraction patterns to determine the type of dislocations in the boundaries. Butler [2] indicated that the boundary dislocations do not have the same Burger's vector as the dislocations within the grains.

To determine Burger's vectors in both the α and β phases, we examined grains extracted during surface replication. These extracted grains were thin enough for high voltage transmission work; by the nature of their formation, they present suitable conditions for examining slip behaviour at room temperature. Normally, in a brittle material like Si_3N_4, the critical stress for dislocation motion is much higher than the fracture stress (at least at low temperatures). Only at the fracture surface do sufficiently high stresses develop to cause dislocation motion. Consequently, the thin extracted grains provided the fracture surfaces for transmission microscopy.

Slip bands observed in α and β grains showed that the dislocations are mostly of the screw type. Tilting experiments, summarized in Table III, indicate that the most common Burger's vector for both α and β is $(c/2)$ [0001]. This has

TABLE III Conditions for dislocation visibility and non-visibility

g	g.b = 0	g.b ≠ 0	Phase
2022		X	β
$3\bar{3}00$	X		β
$02\bar{2}2$		X	β
$2\bar{2}00$	X		β
$10\bar{1}4$		X	α
$20\bar{2}0$	X		α
$10\bar{1}2$		X	α

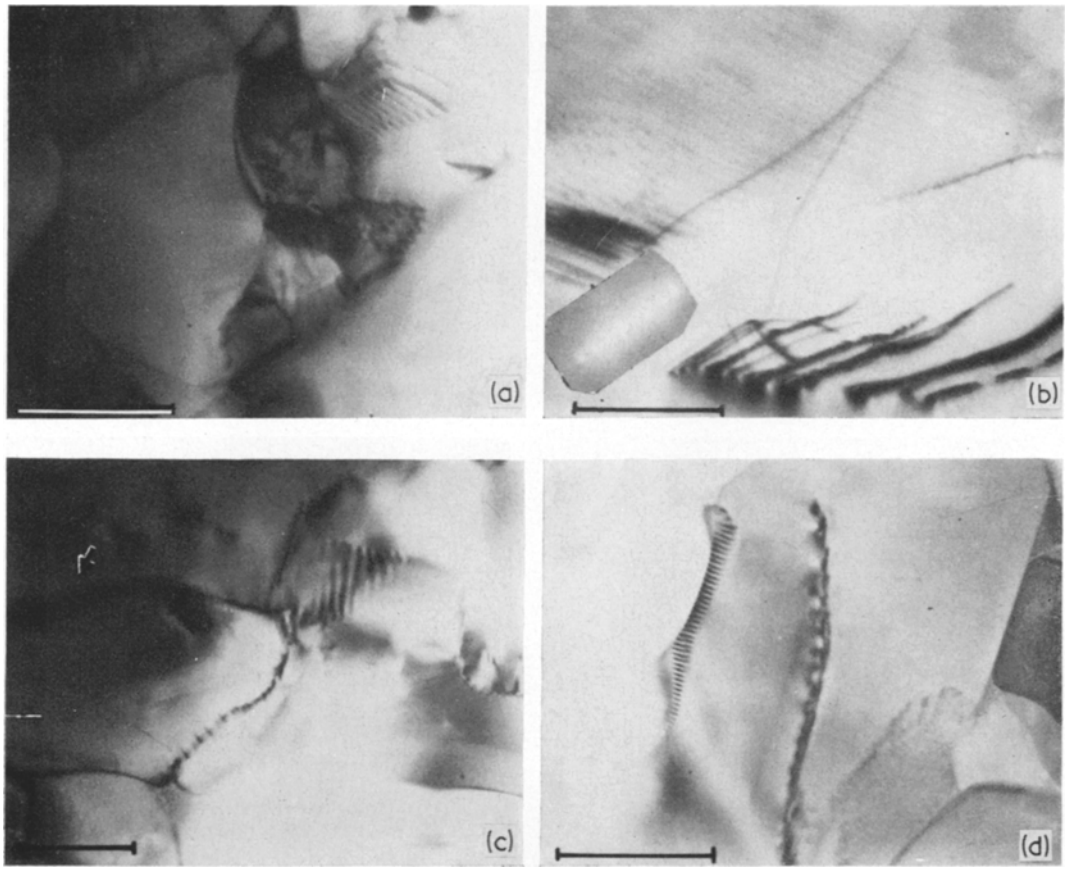

Figure 11 Grain boundary dislocations in hot-pressed Si_3N_4. (a) Hexagonal network. (b) Edge dislocations in a boundary. (c) A twist boundary (arrow). (d) Boundary steps 0.5 μm scale bars.

been observed previously for the β phase only. Thus, from dislocation structures and deformation characteristics, there is no difference between the α and β modifications of Si_3N_4.

4. Discussion

Anisotropy in flexural strength, which decreased with increasing temperatures, was reported [12] and was related to the position of the test specimens with respect to the original billet. Specimens machined with the tensile axis parallel to the hot-pressing direction exhibit lower strength, by about 20%, as compared to specimens cut with the tensile axis perpendicular to the hot-pressing direction. It is unlikely that the low degree of preferred orientation (Fig. 3) can account for the rather significant anisotropy in strength alone.

A lamination effect, which commonly results from restricted powder flow and pressure gradients in pressed powder compacts was demonstrated by the X-ray radiographs. In a bend test on specimens cut with the tensile axis parallel to the hot-pressing direction, the tensile stress is normal to the boundaries between the lamination. Therefore, these specimens would be weaker than those cut in the other direction, where the tensile stress is parallel to the boundaries between laminations.

If we assume that the fracture strength of the material is generally governed by the Griffith relation and, therefore, is inversely proportional to the square root of the critical flaw size, we can show that a lenticular flaw will contribute a different crack size, depending on the orientation of the flaw with respect to the direction of the applied stress. The inclusion shown in the orientation of Fig. 5a is expected to be more critical than that in Fig. 5b. The former is a specimen cut parallel to the hot-pressing direction, while the latter was machined perpendicular to the hot-pressing direction.

Assuming now that the inclusions could define the size of a critical flaw, we apply the Griffith formulation [13] to the three cases in Fig. 4. Although the parameters A, γ, and E in the relation $\sigma = A\sqrt{(\gamma E/c)}$ where c is the critical flaw size, are not known, they remain constant for the three cases, since they define properties of the parent material. Thus we can write

$$\sigma \sqrt{c} = \text{constant} \qquad (2)$$

where σ is the applied stress at the flaw at the moment of failure. The estimated flaw sizes, marked by the two-headed arrows in Fig. 4, are 290, 220 and 140 μm, respectively. The corresponding stresses at the flaw are $\sigma = 276$ MN m^{-2} psi for the silicon particle, located below the surface where the actual stress is lower than that calculated from the overall specimen's dimension; $\sigma = 315$ MN m^{-2} for the iron rich particle and $\sigma = 398$ MN m^{-2} psi for the magnesium rich inclusion. Thus we obtain

TABLE IV

	Particle A	Particle B	Particle C
c(μm)	290	220	140
σ(MN m^{-2})	276	315	398
$\sigma\sqrt{c}$(MN m$^{-3/2}$)	14.9	14.8	14.9

The previous table demonstrates that inclusions, such as shown in Figs. 4 and 5, may be regarded as critical flaws which cause serious degradation in the strength of hot-pressed Si_3N_4.

The Auger and microprobe analyses indicate the existence of other phases in hot-pressed silicon nitride, although the X-ray diffraction data showed traces of Si_2ON_2 only. We can only postulate possible phases and compounds which are consistent with our observations and other recently published data.

4.1. Grain-boundary phases

The high level of oxygen at the boundary (Fig. 6) indicates that the main constituents of the boundary are probably the oxides of Si, Ca, Mg, Al, etc. If we assume that all the oxygen occurs as oxides, we can obtain an upper estimate of the possible composition of the boundary glass phase. The balance of constituents will be:

HS-110 grade: $11SiO_2 \cdot 4.5\ CaO \cdot 1\ MgO \cdot 1\ Al_2O_3$

HS-130 grade: $8\ SiO_2 \cdot 1\ CaO \cdot 1\ MgO$. (3)

The high concentration of CaO in the boundary glass phase is quite significant in that it can account for the substantial difference in high temperature creep strength between the HS-110 and HS-130 grades of Si_3N_4 [14]. Furthermore, the small fluctuations in the level of Ca in the various HS-130 billets, Table I, can account for as much as 25% variation in flexural strengths [15, 16] at 1300°C. Preliminary creep data [14] suggest that a major contribution to the observed deformation comes from grain-boundary sliding. Since the profiles of Ca, K and Na (Fig. 6) indicate substantially higher concentrations in the grain boundary, their effect can be related [14] to an appreciable decrease in the viscosity of silicate glasses with small additions of alkaline oxides [17].

Singhal [18] has constructed thermochemical equilibrium diagrams of the Si-O-N system which show that β-Si_3N_4 and SiO_2 cannot exist as mutually bordering phases. For appropriate partial pressures of N and O, the interface between solid β-Si_3N_4 and SiO_2 is composed of regions of α-Si_3N_4 and Si_2ON_2, respectively. Similar results were obtained by Wild, *et al* [8] Terwilliger and Lange [22] mixed about equal amounts of $MgSiO_3$ and α-Si_3N_4 powders, and melted the mixture at 1700°C. Powder X-ray diffraction of the resulting glass showed strong lines of Mg_2SiO_4 and Si_2ON_2, with no trace of Si_3N_4. Furthermore, the qualitative molecular balance of the compounds in the grain boundary shown above (Equation 3) has at least half of the amount of Si not accounted for (compare with Fig. 6). Finally, the thin foil micrograph, Fig. 1b, shows only few sharp edges and corners in the individual grains. Rounded corners and curved boundaries are strong indications of partial grain dissolution.

We, therefore, propose that during hot-pressing, limited dissolution of β-Si_3N_4 occurs at the glass interface. The boundary glass phase is composed of an inner layer of SiO_2 rich in CaO and MgO, and outer layers of some compound of Si-O-N, probably α-Si_3N_4 and Si_2ON_2.*

*It is interesting to note that if the grain-boundary phase (or phases) were purely amorphous, it would be difficult to account for the grain-boundary dislocations (Fig. 10). However, if the interface between the β-Si_3N_4 grain and the SiO_2 glass phase contains the α-Si_3N_4, high accommodation strains are expected due to the similarity in structure [1] between the two Si_3N_4 phases. The dislocations at the boundary would then be necessary to relax these strains, and they should not have the same structural characteristics as the normal lattice dislocations [19, 20], as was indeed shown by Butler [2].

4.2. Phases within the grain

The Mg traces, Fig. 6, show a persistent level of the element within the grain proper, suggesting that Mg diffuses from the grain boundary during hot-pressing. An examination of densification curves [21] of Si_3N_4 shows that the data can be divided into two portions. An initial, fast rate of densification occurs within the first 15% of the total hot-pressing time, which is followed by a longer period of a much lower rate of densification. The initial portion of the densification curve is probably associated with grain rearrangement as a result of the formation of the liquid phase [22, 23]. Final densification is apparently associated with the concurrent diffusion of Mg from the boundary into the grain, the transformation of α to β and dissolution of the grain at the solid-liquid interface. The accommodation of Mg within the β structure of Si_3N_4 can be achieved by the formation of the $MgSiN_2$ phase [8].

Al can be accommodated in β-Si_3N_4 in appreciable amounts. Oyama [24] has shown that Al_2O_3 is soluble in β-Si_3N_4 in quantities up to 65 mol %, resulting in a very small change in the lattice parameter of β-Si_3N_4. It is not surprising, therefore, that no evidence of Al or Al_2O_3 is indicated by the X-ray diffraction data of either grade of hot-pressed Si_3N_4.

5. Summary and conclusions

1. Ca, Na and K are concentrated at the boundary glass phase in quantities well above the levels indicated by bulk chemical analysis. These impurities are apparently more detrimental to the high temperature strength of Si_3N_4 than any other impurity present.

2. Small pockets, 150 to 300 μm in diameter, of non-densified Si_3N_4 powder occasionally containing small quanties of BN, are frequently found. These inclusions, which have a white, powdery appearance, can be regarded as flaws which cause a substantial decrease in the strength of the material at all temperatures.

3. Fe and W are apparently present as semi-coherent particles within the grains of β-Si_3N_4. These particles are not detrimental to strength.

4. The anisotropy in strength [12] is probably a combined result of banding effects in the hot-pressed billets, the orientation of the lenticular inclusions, and the low degree of preferred orientation.

5. Dislocation characteristics are in agreement with previously reported data [1, 2]. The Burger's vector in α and β phase is $(c/2)$ [0001]. Grain-boundary dislocations are commonly observed.

Acknowledgements

The author is indebted to his colleagues, R. J. Bratton, F. F. Lange, D. G. Miller, G. R. Terwilliger, and S. C. Singhal for stimulating discussions and permission to refer to unpublished data. Technical assistance was rendered by W. J. Carmen (replication), R. W. Palmquist (probe analysis), R. C. Kuznicki (X-ray diffraction), and G. Gidick (spectrographic analysis). The Auger analysis was carried out in co-operation with Dr P. W. Palmberg, Physical Electronic Industries. This work was supported by the Advanced Research Projects Agency, Contract DAAG46-71-C-0162.

References

1. A. G. EVANS and J. V. SHARP, *J. Mater. Sci.* **6** (1971) 1292.
2. E. BUTLER, *Phil. Mag.* **21** (1971) 829.
3. Second Semi-Annual Report, Contract DAA 646-71-C-0162, December, 1972.
4. RAM KOSSOWSKY, *J. Amer. Ceram Soc.* October (1973).
5. F. F. LANGE and G. R. TERWILLIGER, Final Report, Contract N00019-71-C-0107, p. 107.
6. P. W. PALMBERG, Physical Electronics Industries, private communication.
7. S. WILD, P. GRIEVERSON, K. H. JACK and M. J. LATIMER, in "Special Ceramics 5", edited by P. Popper (Brit. Ceram. Res. Assoc., July 1972) p. 377.
8. S. WILD, P. GRIEVERSON and K. H. JACK, *ibid*, p. 286.
9. RAM KOSSOWSKY, paper presented at the Fall meeting of the Basic Science Div., Amer. Ceram. Soc., Philadelphia, September 1972.
10. F. F. LANGE, *Loc. cit.*
11. H. PRIEST, Army Materials and Mechanics Research Center, private communication.
12. First Semi-Annual Report, Contract DAA-G46-71-C-0162, April 1972.
13. R. W. DAVIDGE and A. G. EVANS, *Mat. Sci. Eng.* **6** (1970) 281.
14. RAM KOSSOWSKY and W. C. FRAZIER, paper presented at the Annual Meeting, Amer. Ceram. Soc., Cincinnati, April 1973.
15. RAM KOSSOWSKY, W. C. FRAZIER and F. F. LANGE, *J. Amer. Ceram. Soc.* to be published.
16. D. RICHERSON, paper presented at the Annual Meeting, Amer. Ceram. Soc., Washington, DC, May 1972.
17. R. ROSEN, J. BERSAN and G. URBAIN, *Rev. Hautes Temper et. Refract.* **1** (1964) 159.
18. S. SINGHAL, Westinghouse Research Labs, private communication.

19. H. GLEITER and G. BARO, *Mat. Sci. Eng.* **2** (1967) 224.
20. R. H. HOPKINS and R. KOSSOWSKY, *Acta Metallurgica*, **19** (1971) 203.
21. R. F. COE, R. J. LUMBY and M. F. PAWSON, in "Special Ceramics 5", edited by P. Popper (Brit. Ceram. Res. Assoc., July 1962) p. 361.
22. G. R. TERWILLIGER, and F. F. LANGE, *J. Amer. Ceram. Soc.* to be published.
23. K. H. JACK, paper presented at the Annual Meeting, Amer. Ceram. Soc., Washington, DC, May 1972.
24. YOICHI OYAMA, *Japan J. Appl. Phys.* **11** (1972) 750.

Received 17 April and accepted 4 June 1973.